

STED Nanoscopy Imaging of Cellular Lipid Droplets Employing a Superior Organic Fluorescent Probe

Guannan Liu, Guishan Peng, Jianan Dai, Ri Zhou, Chenguang Wang,* Xu Yan, Xiaoteng Jia, Xiaomin Liu, Yuan Gao,* Lijun Wang, and Geyu Lu



Cite This: *Anal. Chem.* 2021, 93, 14784–14791



Read Online

ACCESS |



Metrics & More

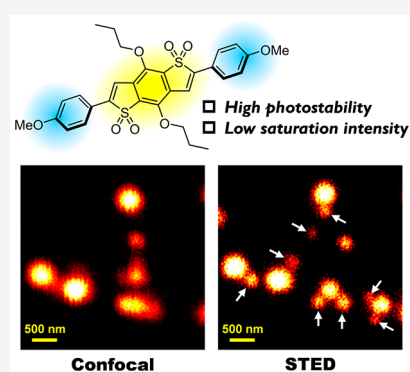


Article Recommendations



Supporting Information

ABSTRACT: Lipid droplets (LDs) are spherical organelles that participate in numerous biological processes. In order to visualize LDs on the nanoscale, nanoscopy fluorescence imaging is considered as the most attractive technique but is substantially limited by the characteristics of fluorescent probes. Thus, the development of a superior fluorescent probe that is capable of nanoscopy fluorescence imaging has attracted enormous attention. Herein, a benzodithiophene-tetraoxide-based molecule Lipi-BDTO has been developed that can easily undergo the stimulated emission depletion (STED) process and displays high photostability. These two characteristics of fluorescent probes finely satisfy the requirements of STED nanoscopy imaging. Indeed, applying the probe for STED imaging achieves a high resolution of 65 nm, belonging to one of the leading results of LDs fluorescence imaging. Furthermore, the high photostability of this fluorescent probe enables it to monitor the dynamics of LDs by time-lapse STED imaging as well as to visualize the three-dimensional (3D) spatial distribution of LDs by 3D STED imaging. Notably, the resolution of the 3D STED image represents one of the best LDs fluorescence imaging results so far. Besides STED nanoscopy imaging, the superior utility of this fluorescent probe has been also demonstrated in two-color 3D confocal imaging and four-color confocal imaging.



Lipid droplets (LDs) are spherical organelles that store neutral lipids, including triglycerides, sterol esters, and retinol esters. Existing in almost all organisms, LDs vary wildly in size depending on the cell type.^{1,2} To be specific, the diameters of LDs are about 10–200 μm in adipocytes, while only 100 nm to 1 μm in adipose tissue. Besides that, the diameters of nascent LDs that are newly generated by release from endoplasmic reticulum (ER) are even less than 100 nm. In recent years, some studies have shown that LDs participate in many critical cellular functions, including lipid storage for energy production and membrane synthesis, virus replication, and protein degradation. Consequently, the study of LDs has become one of the most appealing topics of cell biology in recent years.^{1–5}

In order to visualize LDs and investigate their multiple capabilities, fluorescence imaging techniques (such as wide field, confocal, and two-photon) are generally employed. Therefore, a lot of LDs fluorescent probes have been reported for these fluorescence imaging techniques.^{6–14} Unfortunately, the resolutions of these imaging techniques are intrinsically limited to be about 250 nm (half value of the wavelength) due to light diffraction. Thus, these imaging techniques are not competent for visualizing the small nascent LDs. For this reason, nanoscopy fluorescence imaging techniques, which successfully break the light diffraction limit and provide a significantly higher resolution than 250 nm, have attracted much attention.^{15,16} Among the various nanoscopy imaging

techniques, stimulated emission depletion (STED) microscopy is arguably the most prevalent one, since it provides the highest spatial and temporal resolution.¹⁷

In the case of the STED nanoscopy imaging technique, it has two intrinsic requirements for fluorescent probes: (1) the probe should be able to be efficiently depleted by a STED laser; and (2) the probe should display very high photostability because of the tremendous energy of STED laser.^{18,19} Since the traditional organic fluorescent probes could not satisfy these harsh demands, great efforts have been donated to develop new organic fluorescent probes capable for STED nanoscopy imaging. As a result, a few superior fluorescent probes have been reported very recently for STED nanoscopy imaging of various cellular organelles, e.g., LDs,^{20–25} mitochondrial membrane,^{26–28} cytoskeleton,^{29,30} and so on.^{31–34} Besides these organic molecular fluorescent probes, some organic/inorganic nanoparticles-based fluorescent probes have also emerged as powerful tools for STED imaging.^{35–40} These works highlight the advantage of STED nanoscopy

Received: August 13, 2021

Accepted: October 12, 2021

Published: October 27, 2021



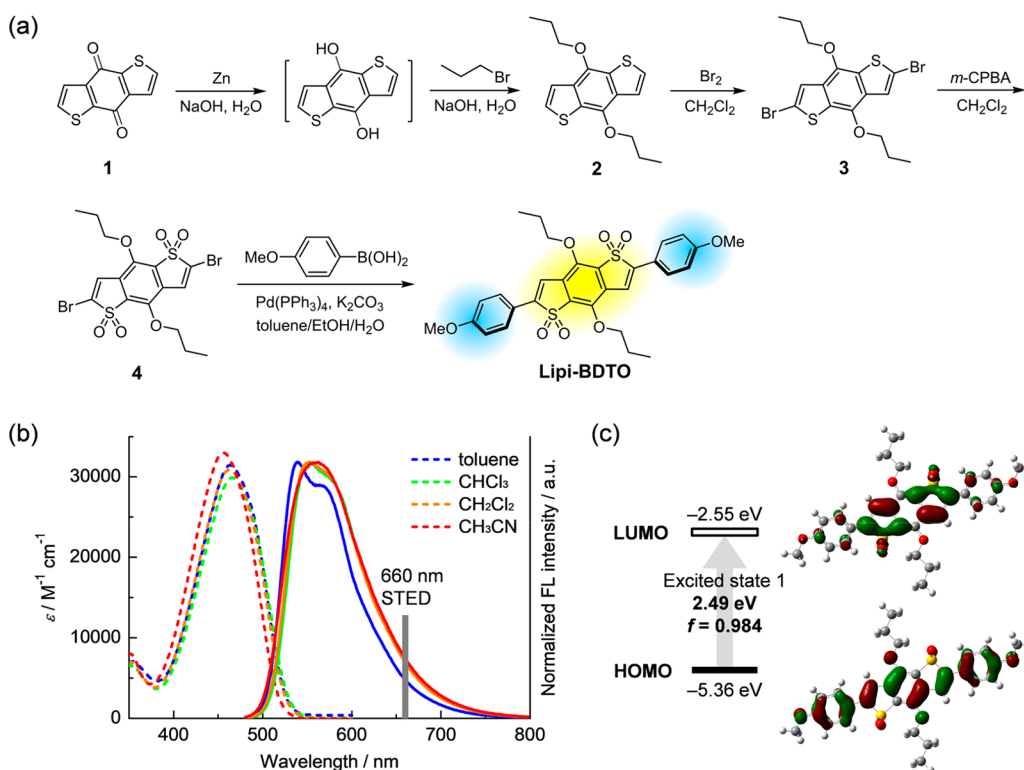


Figure 1. (a) Synthesis of the fluorescent probe Lipi-BDTO. (b) Absorption (dashed line) and fluorescence (solid line) spectra of Lipi-BDTO in various organic solvents. (c) TD-DFT calculation (B3LYP/6-31G*, Gaussian 16) result of Lipi-BDTO: energy diagram, Kohn–Sham HOMO and LUMO, vertical excitation energy, and oscillator strength (f). The first excited state corresponds to the transition of HOMO to LUMO.

imaging over the traditional confocal/two-photon imaging, and significantly promote the relative study of cell biological on the nanoscale. However, fluorescent probes that are competent for STED nanoscopy imaging are quite limited. Moreover, the performances of fluorescent probes, in terms of the depletion efficiency, the resolution, and particularly the photostability under STED imaging, require dramatic improvement.

Herein, we develop a benzodithiophene-tetraoxide-based fluorescent probe named Lipi-BDTO. This novel probe presents outstanding photostability, high fluorescence brightness, good staining specificity toward LDs, and desired cell viability. Moreover, this probe displays a quite low saturation intensity for STED imaging, i.e., this probe can be easily depleted by STED laser. Applying the probe for STED imaging accomplished a very high resolution of 65 nm, belonging to one of the leading results of LDs fluorescence imaging. Consequently, the small nascent LDs which could not be distinguished under confocal imaging had been successfully visualized under STED imaging. Furthermore, the superior photostability of the probe enabled it to be represented in long-term time-lapse STED imaging and 3D STED imaging. Notably, the resolution of the 3D STED image represented one of the best LD fluorescence imaging results so far. Besides STED imaging, the superior utility of this fluorescent probe has also been demonstrated in confocal imaging including two-color 3D confocal imaging as well as four-color confocal imaging.

EXPERIMENTAL SECTION

STED Imaging. Live HeLa cells were stained in DMEM+ containing fluorescent probe Lipi-BDTO (2 μM) and 1% DMSO for 2 h in a CO₂ incubator. Then, the cells were

washed three times with fresh medium to remove the free probes, and kept in HBSS for STED imaging. The Leica TCS SP8 STED system with two continuous wave lasers at 592 and 660 nm for the depletion was used for STED imaging. A HyD detector and a STED WHITE objective (100×/1.40 OIL) were employed. Unless otherwise noted, the STED images were acquired with excitation at 488 nm (WLL), emission in the range of 500–640 nm, and depletion at 660 nm (CW-STED, 16 MW cm⁻²). In general, the images were recorded with a pixel resolution of 22.7 × 22.7 nm², a scan speed of 100 Hz, and a bidirectional model. The images were processed using ImageJ. The full width at half-maximum (fwhm) resolution was determined based on the Gaussian fitting of the signal intensity profiles crossed the LDs.

3D STED Imaging. Live HeLa cells prestained with Lipi-BDTO (2 μM, 2 h) were fixed by 4% paraformaldehyde for 15 min at room temperature. After washing three times with PBS, the cells were kept in PBS for imaging. The Z-stack STED images were recorded with the following set: excitation at 488 nm (WLL), emission in the range of 500–640 nm, depletion at 660 nm (CW-STED, 16 MW cm⁻²), STED-3D factor of 50%, a pixel resolution of 28 × 28 nm², a scan speed of 100 Hz, and a bidirectional model. With a z-step of 50 nm, 103 STED images were recorded in a z-depth of 5.10 μm. Employing Leica LAS X software, the 3D STED image was reconstructed based on the deconvoluted Z-stack STED images.

RESULTS AND DISCUSSION

Molecular Design and Synthesis of Lipi-BDTO. The design of Lipi-BDTO was based on the π-conjugated skeleton consisting of the strong electron-accepting benzodithiophene tetraoxide moiety as the center part and the two weak electron-

Table 1. Photophysical Data for Lipi-BDTO

| solvent | Δf^{a} | λ_{abs} (nm) | ϵ ($\text{M}^{-1} \text{cm}^{-1}$) | λ_{em} (nm) | Stokes shift (nm) | Φ_{F}^b (%) | brightness ($\text{M}^{-1} \text{cm}^{-1}$) | τ (ns) | k_{r} (10^8 s^{-1}) | k_{nr} (10^8 s^{-1}) |
|--------------------------|----------------|-----------------------------|-----------------------------------------------|----------------------------|-------------------|-------------------------|-----------------------------------------------|-------------|------------------------------------------|-------------------------------------------|
| toluene | 0.013 | 463 | 31 500 | 540 | 77 | 98 | 30 900 | 3.54 | 2.8 | 0.06 |
| CHCl_3 | 0.148 | 466 | 29 900 | 552 | 86 | ~ 100 | 29 900 | 4.03 | 2.5 | |
| CH_2Cl_2 | 0.217 | 463 | 30 900 | 551 | 88 | 96 | 29 700 | 3.94 | 2.4 | 0.10 |
| CH_3CN | 0.305 | 456 | 33 000 | 556 | 100 | 84 | 27 700 | 3.93 | 2.1 | 0.41 |

^aThe solvent orientation polarizability. ^bAbsolute fluorescence quantum yield determined by a calibrated integrating sphere system.

donating anisole groups as the terminals (Figure 1a). The thus obtained donor–acceptor–donor-type (D-A-D-type) molecule having weak intramolecular charge transfer (ICT) character in the excited state would display high brightness of fluorescence while ensuring a large Stokes shift. Moreover, the benzodithiophene tetraoxide moiety largely contributes to the high photostability of fluorescent probe due to its strong electron-accepting character. The chemical synthesis of fluorescent probe is straightforward. The detailed procedure has been described in the Supporting Information (SI). The molecular structure of Lipi-DBTO has been fully characterized by NMR and MS spectra, as well as single crystal X-ray diffraction analysis (Figure S4).

Photophysical Property of Lipi-BDTO. The photophysical property of the fluorescent probe Lipi-BDTO has been investigated in organic solvents with various polarities (Figure 1b and Table 1). In solutions, the probe displays strong absorptions with maxima (λ_{abs}) of ~ 465 nm and molar absorption coefficients (ϵ) of $\sim 3.1 \times 10^4 \text{ M}^{-1} \text{ cm}^{-1}$. Therefore, this probe can be efficiently excited by the commonly employed 488 nm laser for bioimaging. Regarding the fluorescence, the probe exhibits intense greenish yellow emissions with maxima (λ_{em}) of ~ 550 nm. Notably, featuring with the large Stokes shifts of 77–100 nm in various solutions, the high fluorescence quantum yields (Φ_{F}) of above 84% are observed for the probe. The fluorescence brightness of probe Lipi-DBTO, as determined by $\epsilon \times \Phi_{\text{F}}$, is about $3.0 \times 10^4 \text{ M}^{-1} \text{ cm}^{-1}$. This value is good in comparison to the well-known and typical LDs fluorescent probe Nile Red ($\sim 2.4 \times 10^4 \text{ M}^{-1} \text{ cm}^{-1}$).⁶

To clarify the superior fluorescence property of the probe, the TD-DFT calculation and the transient fluorescence measurements have been conducted. As shown in Figure 1c, the LUMO of the probe is predominately occupied on the strong electron-accepting benzodithiophene tetraoxide moiety, while the HOMO is delocalized on the entire π -skeleton. The partial separation between LUMO and HOMO would endow the probe with the ICT character, thus displaying the large Stokes shift. Even more, the D-A-D-type π -conjugated framework retains a large oscillator strength of 0.984 between the transition of HOMO \rightarrow LUMO. According to the equation $k_{\text{r}} \propto \nu^2 f$ (where k_{r} represents the radiative decay rate constant, ν represents the wavenumber of the absorption maximum, and f represents the oscillator strength), the radiative process would be very reasonable and the Φ_{F} would be speculated to be high. This inference is verified by the high value of k_{r} (around $2.5 \times 10^8 \text{ s}^{-1}$, Table 1) that is determined based on the fluorescence lifetime (τ) (Figure S5) and Φ_{F} .

LDs Staining Property of Lipi-BDTO. The cellular costaining experiment was initially conducted to reveal the staining specificity of fluorescent probe Lipi-BDTO. A highly specific LDs fluorescent probe Ph-Red was used for the costaining experiment, considering the absorption and

emission spectra.¹⁴ As shown in Figure 2a–c, the two fluorescence imaging channels display good colocalization in

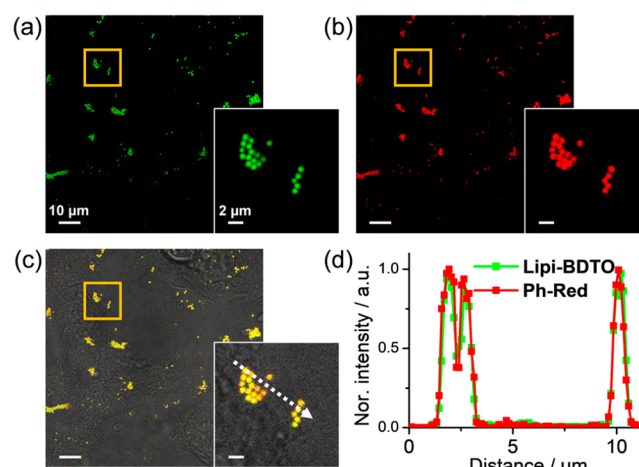


Figure 2. Confocal images of HeLa cells simultaneously labeled with Lipi-BDTO and Ph-Red: (a) Lipi-BDTO; (b) Ph-Red; (c) merge image of (a) and (b) and bright field; scale bar: 10 μm . The enlarged regions are shown in the insets; scale bar: 2 μm . (d) Intensity profiles cross the cells (the dotted lines in the inset).

living HeLa cells. The good overlap of the signal intensity profiles of the two channels further demonstrates the high LDs specificity of this probe (Figure 2d). The Pearson's correlation coefficient (R) value of the two fluorescence channels is 0.85 (Figure S6). Besides HeLa cells, Lipi-BDTO also works well in HepG2 cells with high LDs specificity ($R = 0.86$, Figure S7). Notably, this probe displays high specificity toward LDs in a wide staining concentration range. As shown in Figure S8, the probe Lipi-BDTO could selectively label the ball shape LDs with high specificity in the concentrations of 500 nM–5 μM . In contrast, the significant nonspecific labeling of cellular cytoplasm could be observed for Nile Red that is a representative LDs fluorescent probe.

In addition, the probe Lipi-BDTO displays outstanding photostability. As shown in Figure 3a–c, during continuous confocal imaging under the same excitation conditions, Lipi-BDTO displayed much higher photostability than Nile Red and Ph-Red. After recording 100 confocal images, Lipi-BDTO still maintained 88% fluorescence intensity relative to its initial value, which were dramatically higher than the others (less than 15%) (Figure 3d). The outstanding photostability of probe Lipi-BDTO should be closely in connection with the strong electron-accepting benzodithiophene tetraoxide moiety that largely decreases the HOMO and LUMO levels of molecule. The TD-DFT calculations further support this statement (Figure S9). The decrease of HOMO and LUMO levels of fluorescent probes is in the order of Ph-Red, Nile Red, and Lipi-DBTO, which is consistent with the increasing order of photostability.

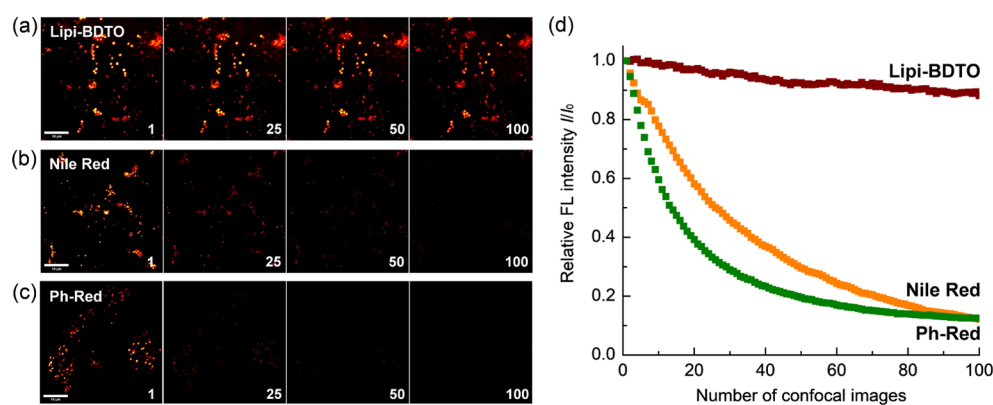


Figure 3. Comparison of the photostability between Lipi-BDTO, Nile Red, and Ph-Red under the same confocal imaging conditions: (a–c) the images of number 1, 25, 50 and 100; scale bar: 10 μm ; and (d) the fluorescence signal intensity of each image (I) relative to the first image (I_0).

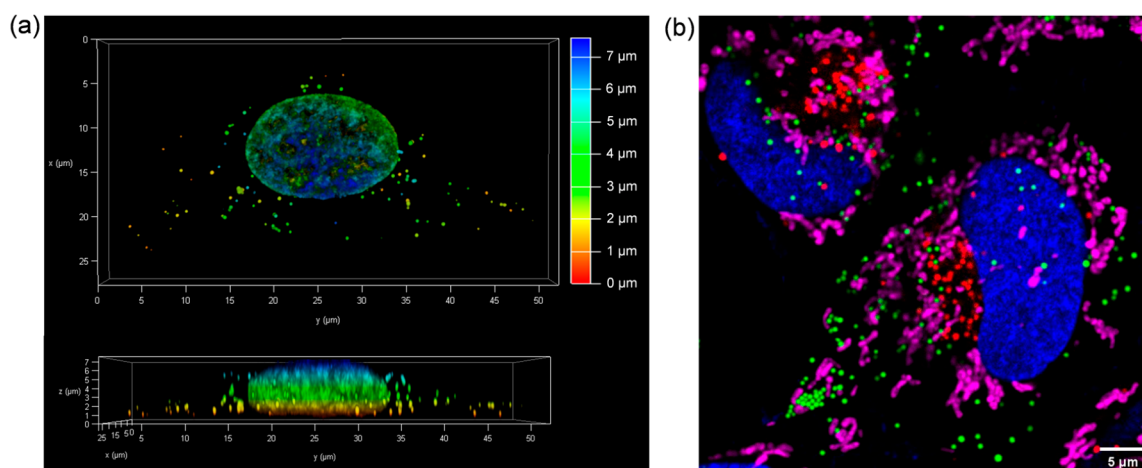


Figure 4. (a) 3D confocal image of fixed HeLa cells labeled with Lipi-BDTO and Hoechst 33342. (b) Multicolor confocal image of living HeLa cells labeled with Hoechst 33342, Lipi-BDTO, LysoTracker Red, and MitoTracker Deep Red, respectively; scale bar: 5 μm .

The emission spectrum of probe Lipi-BDTO in living HeLa cells has been measured (Figure S10). The λ_{em} of ~ 540 nm in cells is comparable to that in toluene solution. This result is reasonable since the components of lipid droplets are quite hydrophobic (low polarity). The cytotoxicity of probe Lipi-BDTO was also assessed by the standard 3-(4,5-dimethylthiazol-2-yl)-2,5-diphenyltetrazolium bromide (MTT) assay. As shown in Figure S11, the viability of HeLa cells will not be affected after being incubated with a concentration up to 10 μM within 24 h. In general, staining cells with Lipi-BDTO in a concentration about 2 μM (2 h) could provide sufficient fluorescence signal. All these results reveal that this probe should be very useful for LDs fluorescence imaging.

3D and Multicolor Confocal Imaging of Lipi-BDTO. In order to demonstrate the superior utility of probe Lipi-BDTO, 3D confocal imaging and multicolor confocal imaging of LDs have been conducted. As a powerful tool, the 3D imaging is highly essential for directly visualizing the dimensional distribution of biological species. Generally, the 3D imaging requires multiple laser scanning of the sample.⁷ Thus, the probe Lipi-BDTO displaying excellent photostability and high brightness of fluorescence is much appreciated for 3D imaging application. The fixed HeLa cells were used for this experiment because the fast displacement of LDs in living cells would significantly reduce the quality of 3D image. The living HeLa cells labeled with probe Lipi-BDTO were fixed with 4%

paraformaldehyde followed by staining with nuclei probe Hoechst 33342. The LDs and nuclei could be imaged in separate channels. Using z-stack slices with a small z-step of 200 nm, the high-quality 3D confocal image was successfully reconstructed (Figure 4a and Movie S1). The full width at half-maximum (fwhm) resolution of the 3D confocal image is 227 ± 7 nm for lateral (xy) plane and 402 ± 17 nm for axial (z) dimension (Figure S12), which is up to the resolution limitation of confocal imaging, demonstrating the good quality of 3D confocal image of LDs.

The multicolor imaging is particularly important for studying the interactions between different biological species.⁷ For this experiment, the cellular organelles nucleus, LDs, lysosomes, and mitochondria were stained with Hoechst 33342, Lipi-BDTO, LysoTracker Red and MitoTracker Deep Red, respectively. The four fluorescent probes could be selectively detected in each imaging channel without cross-talk because of the differences in their spectra (Figure S13). As a result, the multicolor confocal image was successfully obtained, clearly visualizing the various cellular organelles (Figure 4b).

STED Nanoscopy Imaging of Lipi-BDTO. The outstanding photophysical properties and cell imaging features of probe Lipi-BDTO demonstrated its potential application in STED nanoscopy imaging. Primarily, the depletion efficiency of this probe was investigated under the continuous wave depletion laser (CW-STED, 660 nm). The 592 nm depletion

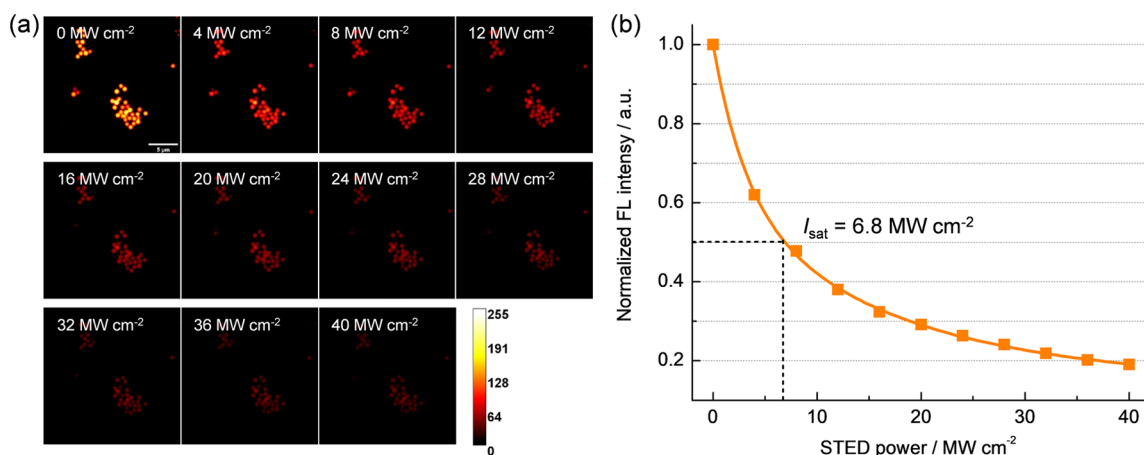


Figure 5. Stimulated emission depletion efficiency of Lipi-BDTO: (a) the fluorescence images of HeLa cells labeled with Lipi-BDTO were recorded under a 488 nm excitation and a 660 nm STED laser (STED laser power of 0 to 40 MW cm^{-2}); scale bar: 5 μm ; (b) the fluorescence signal intensity of each image as a function of the STED laser power.

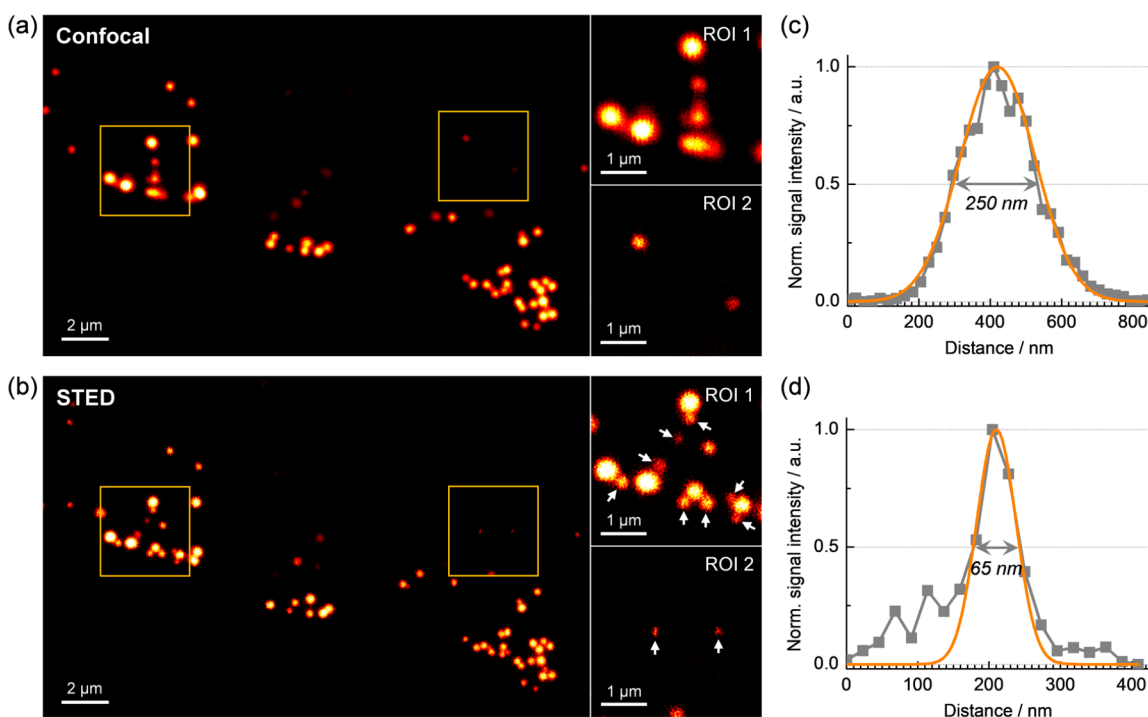


Figure 6. Comparison between (a) confocal image and (b) STED nanoscopy image of HeLa cells labeled with Lipi-BDTO; scale bar: 2 μm . The enlarged regions are shown in the insets; scale bar: 1 μm . Comparison of resolution between (c) confocal and (d) STED image based on the intensity profiles (gray line) crossed the LDs.

laser was not suited for this probe since this laser would directly excite the probe probably due to hot band absorption. As shown in Figure 5a, the fluorescence signals were dramatically depleted when increasing the intensity of STED power. According to the plot of the fluorescence signals, the saturation intensity (I_{sat}) of Lipi-BDTO is determined to be 6.8 MW cm^{-2} (Figure 5b). Notably, this I_{sat} value is quite small and much lower than that of ATTO 647N (10–20 MW cm^{-2}) which is a standard fluorescent probe for STED imaging,^{28,41} also significantly lower than that of the LDs fluorescent probe Lipi-DSB (10.1 MW cm^{-2}) reported by our group very recently.²⁰ This fact means that the probe Lipi-BDTO can achieve a high resolution at a low STED power. The small I_{sat} value should be strongly ascribed to the large Stokes shift

which maintains strong overlap between the 660 nm STED laser and the emission spectrum (a detailed explanation is shown in the SI) while strictly avoiding re-excitation by the STED laser.

Next, STED nanoscopy imaging of this fluorescent probe was studied. The Lipi-BDTO was simultaneously irradiated by a 488 nm excitation laser and a 660 nm STED laser. Thanks to the low I_{sat} value of this probe, a relative weak 660 nm STED laser with intensity of 16 MW cm^{-2} was employed to be able to achieve a sufficiently high resolution. As shown in Figure 6a,b, the STED nanoscopy imaging provides much clearer and sharper LDs than the confocal imaging. Many small LDs which cannot be distinguished under confocal imaging are successfully visualized under STED imaging (insets of Figure 6a,b),

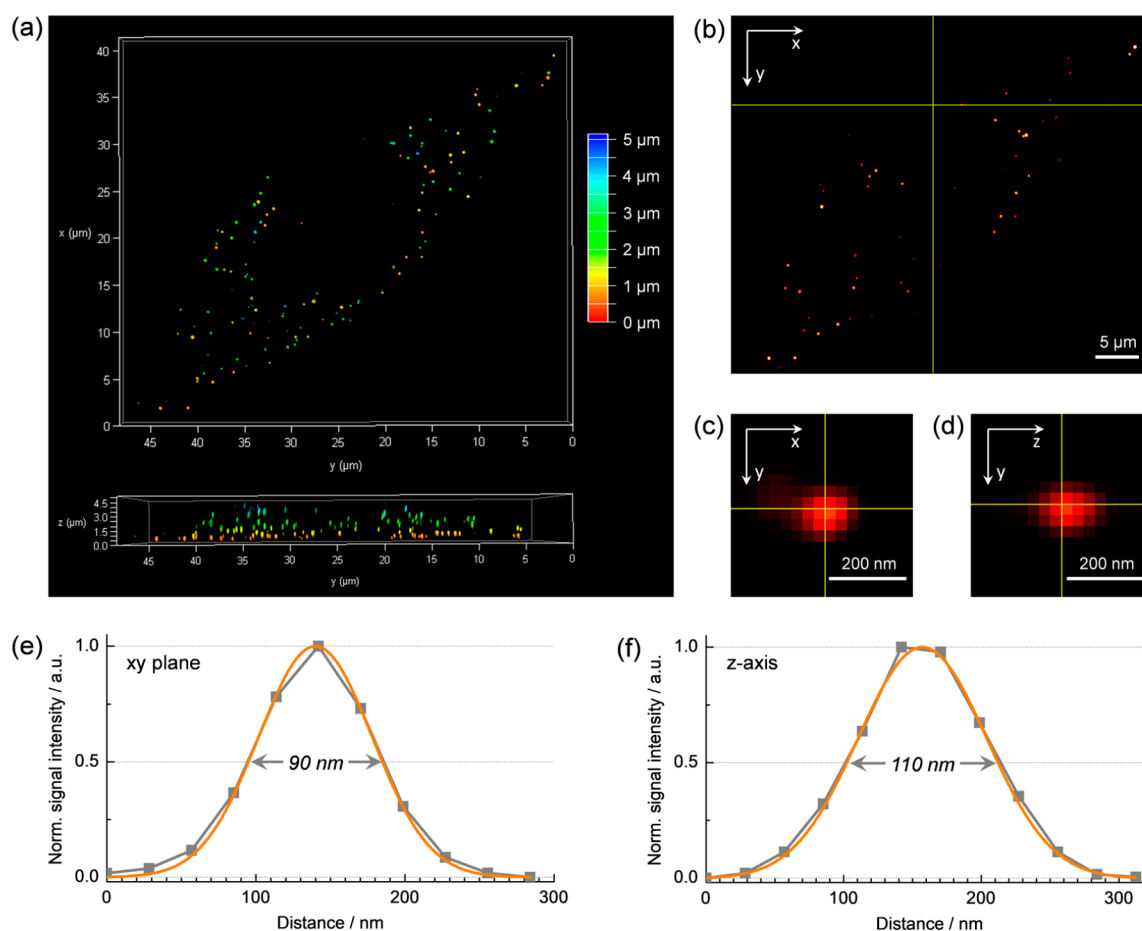


Figure 7. 3D STED nanoscopy image of fixed HeLa cells labeled with Lipi-BDTO. (a) Top and side views of the 3D STED image. (b–d) Orthogonal view (xy and yz planes) of LDs. (e,f) The fluorescence signal intensity profiles (gray line) crossed the LDs.

highlighting the advantage and utility of STED imaging with this fluorescent probe. The fwhm resolution of the STED image is up to 65 ± 7 nm, which is substantially higher than the confocal image of 250 ± 6 nm (Figure 6c,d) and belongs to one of the leading results of LDs imaging (Table S1).^{20–25} Notably, this high-resolution STED image is obtained under a relative weak STED laser intensity (16 MW cm^{-2}), which is highly desired for live cell imaging with decreased photo-damage. Further enhancing the fwhm resolution better than 65 nm may be realized by STED imaging with time-gated detection.

Importantly, the superior photostability ensures that the probe can be explored in time-lapse STED nanoscopy imaging. As shown in Figure S14 and Movie S2, the long-term dynamics of LDs in living HeLa cells were successfully recorded over 200 frames (262 s) under a STED power of 16 MW cm^{-2} , while still maintaining 70% of its initial fluorescence signal. This is an exciting result because the powerful STED laser usually induces dramatic photobleaching of the fluorescence signal. Only very few state-of-the-art organic fluorescent probes are capable for long-term time-lapse STED imaging (Table S2).

The high photostability further enabled Lipi-BDTO to be explored in 3D STED nanoscopy imaging. Similar to the 3D confocal image as before mentioned, the 3D STED nanoscopy image was also commonly obtained by multiple laser scanning and then reconstructing the z -stack images. However, the 3D STED image is much more challenging because of the serious photobleaching of fluorescent probes during multiple STED

imaging scans of the sample.^{30,42} For this experiment, under a STED laser intensity of 16 MW cm^{-2} , the high-quality 3D STED image was successfully reconstructed using z -stack slices with a small z -step of 50 nm (Figure 7a and Movie S3). The resolution of the 3D STED image is 90 ± 1 nm for the lateral (xy) plane and 110 ± 2 nm for the axial (z) dimension (Figure 7b–f), which is substantially higher than the 3D confocal image (227 nm for lateral plane, 402 nm for axial dimension). The spatial resolution of the 3D STED image ($90 \times 90 \times 110 \text{ nm}^3$) is improved 23 \times in comparison to the confocal image, implying that the 3D distribution of LDs can be much more clearly distinguished. Moreover, the spatial resolution represents one of the best results of LDs imaging to date (Table S1) and is comparable to or even better than other cellular organelles stained with organic fluorescent probes (Table S2).^{28,30}

CONCLUSIONS

We have developed a novel fluorescent probe Lipi-BDTO which displays high photostability and low saturation intensity. These features finely satisfy the requirements of STED nanoscopy imaging, e.g., time-lapse STED imaging and 3D STED imaging. Therefore, the cellular LDs have been precisely visualized by STED imaging with nanoscale resolution, which is substantially higher than the traditional confocal imaging and represents one of the leading results of LDs fluorescence imaging so far. Besides STED imaging, the superior utility of this fluorescent probe has also been demonstrated in two-color

3D confocal imaging as well as four-color confocal imaging. Studies employing the fluorescent probe as a powerful tool to discover the new biological process of LDs on the nanoscale are ongoing by our group and our collaborators.

■ ASSOCIATED CONTENT

Supporting Information

The Supporting Information is available free of charge at <https://pubs.acs.org/doi/10.1021/acs.analchem.1c03474>.

Chemical synthesis and characterization data of all new compounds, additional fluorescence imaging data, and MTT assay results (PDF)

Two-color 3D confocal imaging (AVI)

Time-lapse STED imaging (AVI)

3D STED imaging (AVI)

■ AUTHOR INFORMATION

Corresponding Authors

Chenguang Wang – State Key Laboratory of Integrated Optoelectronics, Key Laboratory of Advanced Gas Sensors of Jilin Province, College of Electronic Science & Engineering, Jilin University, Changchun 130012, People's Republic of China; orcid.org/0000-0001-9770-1062; Email: wangchenguang@jlu.edu.cn

Yuan Gao – State Key Laboratory of Integrated Optoelectronics, Key Laboratory of Advanced Gas Sensors of Jilin Province, College of Electronic Science & Engineering, Jilin University, Changchun 130012, People's Republic of China; Email: gaoyuan@jlu.edu.cn

Authors

Guannan Liu – State Key Laboratory of Integrated Optoelectronics, Key Laboratory of Advanced Gas Sensors of Jilin Province, College of Electronic Science & Engineering, Jilin University, Changchun 130012, People's Republic of China

Guishan Peng – State Key Laboratory of Integrated Optoelectronics, Key Laboratory of Advanced Gas Sensors of Jilin Province, College of Electronic Science & Engineering, Jilin University, Changchun 130012, People's Republic of China

Jianan Dai – State Key Laboratory of Integrated Optoelectronics, Key Laboratory of Advanced Gas Sensors of Jilin Province, College of Electronic Science & Engineering, Jilin University, Changchun 130012, People's Republic of China

Ri Zhou – State Key Laboratory of Integrated Optoelectronics, Key Laboratory of Advanced Gas Sensors of Jilin Province, College of Electronic Science & Engineering, Jilin University, Changchun 130012, People's Republic of China

Xu Yan – State Key Laboratory of Integrated Optoelectronics, Key Laboratory of Advanced Gas Sensors of Jilin Province, College of Electronic Science & Engineering, Jilin University, Changchun 130012, People's Republic of China; orcid.org/0000-0003-2152-675X

Xiaoteng Jia – State Key Laboratory of Integrated Optoelectronics, Key Laboratory of Advanced Gas Sensors of Jilin Province, College of Electronic Science & Engineering, Jilin University, Changchun 130012, People's Republic of China; orcid.org/0000-0001-5630-8838

Xiaomin Liu – State Key Laboratory of Integrated Optoelectronics, Key Laboratory of Advanced Gas Sensors of

Jilin Province, College of Electronic Science & Engineering, Jilin University, Changchun 130012, People's Republic of China; orcid.org/0000-0003-4186-9637

Lijun Wang – State Key Laboratory of Integrated Optoelectronics, Key Laboratory of Advanced Gas Sensors of Jilin Province, College of Electronic Science & Engineering, Jilin University, Changchun 130012, People's Republic of China; State Key Laboratory of Luminescence and Applications, Changchun Institute of Optics, Fine Mechanics and Physics, Chinese Academy of Sciences, Changchun 130033, People's Republic of China

Geyu Lu – State Key Laboratory of Integrated Optoelectronics, Key Laboratory of Advanced Gas Sensors of Jilin Province, College of Electronic Science & Engineering, Jilin University, Changchun 130012, People's Republic of China; orcid.org/0000-0002-7428-2456

Complete contact information is available at:

<https://pubs.acs.org/doi/10.1021/acs.analchem.1c03474>

Author Contributions

All authors have given approval to the final version of the manuscript.

Notes

The authors declare no competing financial interest.

■ ACKNOWLEDGMENTS

This work is supported by the National Nature Science Foundation of China (61831011 and 62075079), the China Postdoctoral Science Foundation (2019T120238, 2018M640282, 2020M670847, and 2020T130239), the Natural Science Foundation of Jilin Province (20200201289JC), and Science and Technology Project of Jilin Provincial Department of Education (JJKH20200982KJ).

■ REFERENCES

- (1) Olzmann, J. A.; Carvalho, P. *Nat. Rev. Mol. Cell Biol.* **2019**, *20*, 137–155.
- (2) Thiam, A. R.; Beller, M. *J. Cell Sci.* **2017**, *130*, 315–324.
- (3) Farese, R. V., Jr.; Walther, T. C. *Cell* **2009**, *139*, 855–860.
- (4) Thiam, A. R.; Farese, R. V., Jr.; Walther, T. C. *Nat. Rev. Mol. Cell Biol.* **2013**, *14*, 775–786.
- (5) Walther, T. C.; Farese, R. V., Jr. *Annu. Rev. Biochem.* **2012**, *81*, 687–714.
- (6) Fam, T. K.; Klymchenko, A. S.; Collot, M. *Materials* **2018**, *11*, 1768.
- (7) Collot, M.; Fam, T. K.; Ashokkumar, P.; Faklaris, O.; Galli, T.; Danglot, L.; Klymchenko, A. S. *J. Am. Chem. Soc.* **2018**, *140*, 5401–5411.
- (8) Guo, L.; Tian, M.; Zhang, Z.; Lu, Q.; Liu, Z.; Niu, G.; Yu, X. *J. Am. Chem. Soc.* **2021**, *143*, 3169–3179.
- (9) Zhang, X.; Yuan, L.; Jiang, J.; Hu, J.; du Rietz, A.; Cao, H.; Zhang, R.; Tian, X.; Zhang, F.; Ma, Y.; Zhang, Z.; Uvdal, K.; Hu, Z. *Anal. Chem.* **2020**, *92*, 3613–3619.
- (10) Jiang, G.; Jin, Y.; Li, M.; Wang, H.; Xiong, M.; Zeng, W.; Yuan, H.; Liu, C.; Ren, Z.; Liu, C. *Anal. Chem.* **2020**, *92*, 10342–10349.
- (11) Wang, K.; Ma, S.; Ma, Y.; Zhao, Y.; Xing, M.; Zhou, L.; Cao, D.; Lin, W. *Anal. Chem.* **2020**, *92*, 6631–6636.
- (12) Fan, L.; Wang, X.; Zan, Q.; Fan, L.; Li, F.; Yang, Y.; Zhang, C.; Shuang, S.; Dong, C. *Anal. Chem.* **2021**, *93*, 8019–8026.
- (13) Liu, M.; Ding, N.; Chen, S.; Yu, Y.; Wang, J. *Anal. Chem.* **2021**, *93*, 5284–5290.
- (14) Zhou, R.; Cui, Y.; Dai, J.; Wang, C.; Liang, X.; Yan, X.; Liu, F.; Liu, X.; Sun, P.; Zhang, H.; Wang, Y.; Lu, G. *Adv. Opt. Mater.* **2020**, *8*, 1902123.

- (15) Sahl, S. J.; Hell, S. W.; Jakobs, S. *Nat. Rev. Mol. Cell Biol.* **2017**, *18*, 685–701.
- (16) Sigal, Y. M.; Zhou, R.; Zhuang, X. *Science* **2018**, *361*, 880–887.
- (17) Vicidomini, G.; Bianchini, P.; Diaspro, A. *Nat. Methods* **2018**, *15*, 173–182.
- (18) Wang, L.; Frei, M. S.; Salim, A.; Johnsson, K. *J. Am. Chem. Soc.* **2019**, *141*, 2770–2781.
- (19) Liu, Z.; Liu, J.; Wang, X.; Mi, F.; Wang, D.; Wu, C. *Bioconjugate Chem.* **2020**, *31*, 1857–1872.
- (20) Zhou, R.; Wang, C.; Liang, X.; Liu, F.; Yan, X.; Liu, X.; Sun, P.; Zhang, H.; Wang, Y.; Lu, G. *ACS Materials Lett.* **2021**, *3*, 516–524.
- (21) Taki, M.; Kajiwara, K.; Yamaguchi, E.; Sato, Y.; Yamaguchi, S. *ACS Materials Lett.* **2021**, *3*, 42–49.
- (22) Liu, X.; Lu, X.; Zhu, T.; Wenli, D.; Zhenghui, Y.; Cao, H.; Wang, S.; Tian, Y.; Zhang, Z.; Zhang, R.; De Souza, S. C.; Tian, X. *Biosens. Bioelectron.* **2021**, *175*, 112871.
- (23) Xu, Y.; Zhang, H.; Zhang, N.; Xu, R.; Wang, Z.; Zhou, Y.; Shen, Q.; Dang, D.; Meng, L.; Tang, B. *Z. Mater. Chem. Front.* **2021**, *5*, 1872–1883.
- (24) Xu, H.; Zhang, H.; Liu, G.; Kong, L.; Zhu, X.; Tian, X.; Zhang, Z.; Zhang, R.; Wu, Z.; Tian, Y.; Zhou, H. *Anal. Chem.* **2019**, *91*, 977–982.
- (25) O'Connor, D.; Byrne, A.; Berselli, G. B.; Long, C.; Keyes, T. E. *Analyst* **2019**, *144*, 1608–1621.
- (26) Wang, C.; Taki, M.; Sato, Y.; Tamura, Y.; Yaginuma, H.; Okada, Y.; Yamaguchi, S. *Proc. Natl. Acad. Sci. U. S. A.* **2019**, *116*, 15817–15822.
- (27) Stephan, T.; Roesch, A.; Riedel, D.; Jakobs, S. *Sci. Rep.* **2019**, *9*, 12419.
- (28) Yang, X.; Yang, Z.; Wu, Z.; He, Y.; Shan, C.; Chai, P.; Ma, C.; Tian, M.; Teng, J.; Jin, D.; Yan, W.; Das, P.; Qu, J.; Xi, P. *Nat. Commun.* **2020**, *11*, 3699.
- (29) Lukinavicius, G.; Reymond, L.; D'Este, E.; Masharina, A.; Gottfert, F.; Ta, H.; Guthier, A.; Fournier, M.; Rizzo, S.; Waldmann, H.; Blaukopf, C.; Sommer, C.; Gerlich, D. W.; Arndt, H.-D.; Hell, S. W.; Johnsson, K. *Nat. Methods* **2014**, *11*, 731–733.
- (30) Wang, C.; Taki, M.; Sato, Y.; Fukazawa, A.; Higashiyama, T.; Yamaguchi, S. *J. Am. Chem. Soc.* **2017**, *139*, 10374–10381.
- (31) Bottanelli, F.; Kromann, E. B.; Allgeyer, E. S.; Erdmann, R. S.; Wood Baguley, S.; Sirinakakis, G.; Schepartz, A.; Baddeley, D.; Toomre, D. K.; Rothman, J. E.; Bewersdorf, J. *Nat. Commun.* **2016**, *7*, 10778.
- (32) Spahn, C.; Hurter, F.; Glaesmann, M.; Karathanasis, C.; Lampe, M.; Heilemann, M. *Angew. Chem., Int. Ed.* **2019**, *58*, 18835–18838.
- (33) Spahn, C.; Grimm, J. B.; Lavis, L. D.; Lampe, M.; Heilemann, M. *Nano Lett.* **2019**, *19*, 500–505.
- (34) Wang, C.; Taki, M.; Kajiwara, K.; Wang, J.; Yamaguchi, S. *ACS Materials Lett.* **2020**, *2*, 705–711.
- (35) Man, Z.; Cui, H.; Lv, Z.; Xu, Z.; Wu, Z.; Wu, Y.; Liao, Q.; Liu, M.; Xi, P.; Zheng, L.; Fu, H. *Nano Lett.* **2021**, *21*, 3487–3494.
- (36) Wu, Y.; Ruan, H.; Dong, Z.; Zhao, R.; Yu, J.; Tang, X.; Kou, X.; Zhang, X.; Wu, M.; Luo, F.; Yuan, J.; Fang, X. *Anal. Chem.* **2020**, *92*, 12088–12096.
- (37) Li, D.; Qin, W.; Xu, B.; Qian, J.; Tang, B. *Z. Adv. Mater.* **2017**, *29*, 1703643.
- (38) Fang, X.; Chen, X.; Li, R.; Liu, Z.; Chen, H.; Sun, Z.; Ju, B.; Liu, Y.; Zhang, S. X.-A.; Ding, D.; Sun, Y.; Wu, C. *Small* **2017**, *13*, 1702128.
- (39) Liu, Y.; Lu, Y.; Yang, X.; Zheng, X.; Wen, S.; Wang, F.; Vidal, X.; Zhao, J.; Liu, D.; Zhou, Z.; Ma, C.; Zhou, J.; Piper, J.; Xi, P.; Jin, D. *Nature* **2017**, *543*, 229–233.
- (40) Ye, S.; Yan, W.; Zhao, M.; Peng, X.; Song, J.; Qu, J. *Adv. Mater.* **2018**, *30*, 1800167.
- (41) Liu, Y.; Ding, Y.; Alonas, E.; Zhao, W.; Santangelo, P. J.; Jin, D.; Piper, J. A.; Teng, J.; Ren, Q.; Xi, P. *PLoS One* **2012**, *7*, No. e40003.
- (42) Wildanger, D.; Medda, R.; Kastrop, L.; Hell, S. W. *J. Microsc.* **2009**, *236*, 35–43.